Flat-band exciton in two-dimensional Kagomé quantum wire systems

Hiroyuki Ishii* and Takashi Nakayama†
Department of Physics, Chiba University, 1-33 Yayoi, Inage, Chiba 263-8522, Japan

Jun-ichi Inoue‡
Center for Frontier Science, Chiba University, 1-33 Yayoi, Inage, Chiba 263-8522, Japan
(Received 21 August 2003; published 27 February 2004)

Exciton states in the two-dimensional Kagomé lattice, which is fabricated by the semiconductor quantum wires and has the electronic band structure with dispersionless flat bands, are studied theoretically using the tight-binding model. It is found that the binding energy of an exciton in the Kagomé lattice is larger than the exciton binding energies in other two-dimensional lattices and even larger than that in the one-dimensional lattice. It is shown that such large binding energy originates from the macroscopic degree of degeneracy and the localized nature of the flat-band states in the Kagomé lattice. This large binding energy is controllable by applying an external magnetic field. Furthermore, contrary to the exciton state, we also show that both the binding energy of a charged exciton and that of a biexciton in the Kagomé lattice are much smaller than those in other lattices.

DOI: 10.1103/PhysRevB.69.085325 PACS number(s): 73.21.−b, 78.67.−n

I. INTRODUCTION

The recent progress in the field of nanotechnology has made it possible to fabricate semiconductor quantum wires with nanoscale width and to arrange them at arbitrary positions on the semiconductor surfaces. Since the electrons and/or holes are mainly confined in the quantum wires, the periodic arrangement of quantum wires provides ideal two-dimensional lattice-network systems. These artificial lattices have advantages over the conventional bulk crystals; for example, the number of electrons are controlled by varying the gate voltage connected to the substrate and the lattices do not undergo the structural deformation, such as the Jahn-Teller distortion, upon carrier doping. In this way, the quantum-wire artificial lattice systems provide new stages for physical phenomena.

Electronic structures of lattice systems have been studied theoretically for a long time. In 1976, Hofstader showed that the two-dimensional lattice systems give fractal energy spectra with an external magnetic field.[1] This theoretical result has been confirmed by Albrecht *et al*. experimentally using the quantum-wire systems.[2] One of the recent important subjects concerning the lattice systems is flat-band ferromagnetism. Mielke and Tasaki showed by using the Hubbard model that the Kagomé lattice has a complete flat electronic band and shows a ferromagnetic behavior when the flat band is half filled with electrons.[3,4] The local spin-density functional calculation based on the effective-mass approximation also showed that the surface ferromagnetism appears on the InAs Kagomé quantum-wire system when the flat band is half filled.[4,5] Motivated by these theoretical predictions, the experimental challenge to realize the Kagomé lattice is now in progress.[6]

Currently, a variety of lattice systems are known to have electronic flat bands. Among these systems, there are common features. (i) A flat band exists as a pair with dispersive bands, reflecting the multisites in the unit cell. Using the specific geometry of site connection in lattices, one can delete the wave-function amplitude on the sites around one unit cell and can choose eigenstates of a flat band as completely localized around one unit cell. (ii) Since each unit cell has a localized eigenstate, a sum of such eigenstates becomes a complete set of flat-band states, with the same eigenenergy, producing the macroscopic degree of degeneracy. (iii) The above-mentioned localized states are nonorthogonal and have finite overlaps with each other. This indicates that when one produces the Wannier functions of a flat band, they are not localized. These features, i.e., the localization, macroscopic degree of degeneracy, and nonorthogonal features of flat-band eigenstates, are closely related to the appearance of ferromagnetism. We can expect that these unique features also promote exotic optical properties in flat-band lattice systems, which have never been studied so far. This is the motivation of the present work.

In the previous paper, we briefly reported the theoretical results of the exciton properties in the Kagomé lattice by using the simple mathematical tight-binding model.[7,8] In this paper, we extend this work by considering realistic situations of the InAs Kagomé quantum-wire system and other lattice systems, and analyze in detail the origin of unique exciton features in the Kagomé lattice. The most remarkable finding of the present study is that the binding energy of an exciton in the Kagomé lattice is larger than that in the one-dimensional system, contrary to the well-known result that the binding energies of excitons in high-dimension systems are smaller than those in low-dimension systems. Since the exciton is associated with the flat bands in the Kagomé lattice, we call this exotic exciton as a flat-band exciton in this paper.

The rest of this paper is organized as follows. In Sec. II, the model of the InAs Kagomé quantum-wire lattice and the calculation method are described. In Sec. III, the binding energy and the wave function of the flat-band exciton are first discussed, and compared with those of other lattice systems. Next, the origin of the large binding energy of a flat-band exciton is analyzed using a perturbation method. It is

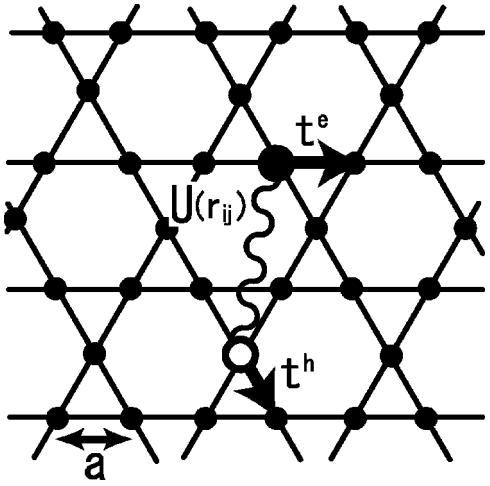

FIG. 1. Tight-binding model for exciton state in the Kagomé quantum-wire system. An electron in a conduction band (large solid circle) and a hole in the valence band (large open circle) locate at the cross points of quantum wires, and transfer between two nearest-neighbor cross points as shown by arrows. The Coulomb attractive interaction $U(r_{ij})$ works between an electron and a hole.

shown here that both the localization and degeneracy natures of flat-band electronic states promote the large binding energy. Then, the variation of the binding energy with magnetic field and the stability of the flat-band exciton are studied, by calculating the binding energies of charged excitons and biexcitons. Section IV concludes the paper.

II. MODEL AND METHOD

We investigate the Kagomé quantum-wire system, where the quantum wires are made of InAs and surrounded by $In_{0.72}Ga_{0.28}As$ barrier regions. The width of quantum wires is 10.4 nm, and the lattice constant is 72 nm. A system of this size can be produced by recent nanotechnology.[6] Local spin-density approximation calculation for this system shows that the electron density localizes at the cross points of the quantum wires.[5,9] A similar result is obtained for the hole density because InAs quantum wires also work to confine holes. Therefore, we assume that the electronic structures of electrons and holes in the lower conduction and higher valence bands are well described by employing the tight-binding model, where electrons and holes are located at the cross points of quantum wires and transfer along the wires. This situation is schematically shown in Fig. 1. Moreover, an electron and a hole are assumed to be other kinds of fermions, for simplicity.[10] Under these assumptions, the model Hamiltonian of the system becomes

$$\hat{\mathcal{H}}=\sum_{\langle i,j\rangle} t_{ij}^{e}\hat{a}_i^{\dagger}\hat{a}_j+\sum_{\langle i,j\rangle} t_{ij}^{h}\hat{b}_i^{\dagger}\hat{b}_j+\sum_{i,j} U(r_{ij})\hat{a}_i^{\dagger}\hat{a}_i\hat{b}_j^{\dagger}\hat{b}_j, \quad (1)$$

where $\hat{a}_i$ and $\hat{b}_i$, respectively, represent the annihilation operators of an electron and a hole at the ith cross point of quantum wires. t_{ij}^{e} and t_{ij}^{h} are transfer energies of an electron and a hole from the ith to the jth cross points, respectively. The summation $\langle i,j\rangle$ runs over the entire nearest-neighbor cross-point pairs. $U(r_{ij})$ is the Coulomb attraction energy between an electron and a hole, for which we employ the form[10,11]

$$U(r_{ij})=\begin{cases} -U_0 & \text{for} \quad i=j \\ -\dfrac{0.75U_0}{(r_{ij}/a)} & \text{for} \quad i\neq j, \end{cases} \quad (2)$$

where r_{ij} is the distance between the i and jth cross points a represents the distance between the nearest-neighbor cross points of quantum wires evaluated as 36 nm. The employment of this form of Coulomb energy is equivalent to the introduction of the cutoff parameter in one-dimensional systems to avoid the divergence of the eigenvalue of the Hamiltonian (1) and corresponds to the screening around the on-site.[10,11] The band-gap energy between the valence band and the conduction band has an arbitrary value in our model.

We must estimate the transfer energies, t^e and t^h, and the on-site Coulomb energy, U_0, for the InAs Kagomé lattice on the semiconductor surface to evaluate the exciton binding energy. The local-density approximation calculation shows that the total width of the conduction bands is about 10 meV,[9] while the corresponding bandwidth by the present model is $6t^e$. Therefore, we are able to take the electron transfer energy t^e as 1.67 meV. Note that since the lowest-energy state at the cross point has the s-like orbital, the s-s coupling between the nearest sites gives a negative value to the electron transfer energy t^e in most cases. However, as shown in Sec. III D, the sign of t^e is easily changed by applying a magnetic field to the lattice system. Thus, in this paper, we assume that t^e has a positive value. In this case, the flat band appears as the lowest conduction band. We approximate the hole transfer energy t^h equal to the electron transfer energy t^e for simplicity. This is because the reduced mass of an electron and a hole in InAs is almost equal to the effective mass of an electron. On the other hand, when an electron and a hole are located at nearest-neighbor sites, the Coulomb attraction energy between them is $-e^2/4\pi\varepsilon a$, where ε represents the relative dielectric constant of InAs, $\varepsilon=12.4$, and e is the elementary electric charge. Thus, the on-site Coulomb energy U_0 is estimated as 4.18 meV.

The exciton states are obtained as the lowest-energy bound eigenstates of the Hamiltonian. The exciton binding energy E_B is calculated as

$$E_B=E(U_0=0)-E(U_0\neq 0), \quad (3)$$

where $E(U_0=0)$ and $E(U_0\neq 0)$ are the lowest eigenvalues of the Hamiltonian without and with the Coulomb attraction interaction, respectively. The Hamiltonian is numerically diagonalized by the Lanchos method for Kagomé lattices of finite size as large as 15×15 unit cells with periodic boundary conditions. To check the convergence of the calculated binding energy of exciton, we varied the size of the system and confirmed that the binding energy of an exciton is obtained with 1% accuracy in the present calculation.

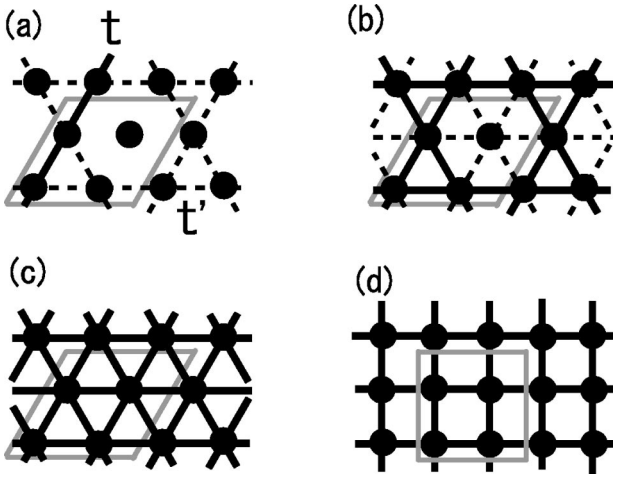

FIG. 2. The lattice models adopted in this work: (a) one-dimensional, (b) Kagomé, (c) triangle, and (d) square lattices. Unit cells of these lattices are shown in (a)–(d) by gray square frames. Kagomé and triangle lattices are obtained from one-dimensional and Kagomé lattices, respectively, by allowing the carrier transfer along broken lines in (a) and (b).

III. RESULTS AND DISCUSSION

A. Binding energy and exciton Bohr radius

First, we consider the exciton binding energy in the Kagomé lattice. In order to clarify the characteristics of the Kagomé system, we compare binding energies among various lattice systems. Schematic diagrams of one-dimensional, two-dimensional Kagomé, triangle and square lattices are shown in Figs. 2(a)–2(d) as solid lines, respectively. Unit cells of these lattices are also represented by gray square frames in Figs. 2(a)–2(d). The calculated electron and hole band structures of these lattices are shown in Figs. 3(a)–3(d). As shown in Fig. 3(b), the flat bands appear as the lowest conduction and the highest valence bands for the Kagomé lattice.

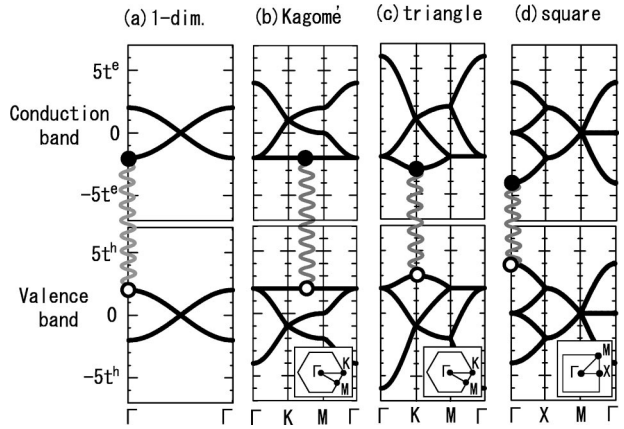

FIG. 3. The electronic band structure of (a) one-dimensional, (b) Kagomé, (c) triangle, and (d) square lattices. Solid and open circles represent an electron state at the bottom of the conduction band and a hole state at the top of the valence band, respectively, and the wavy lines schematically indicate the Coulomb attraction interactions. Insets are the Brillouin zones corresponding to the unit cells in Fig. 2.

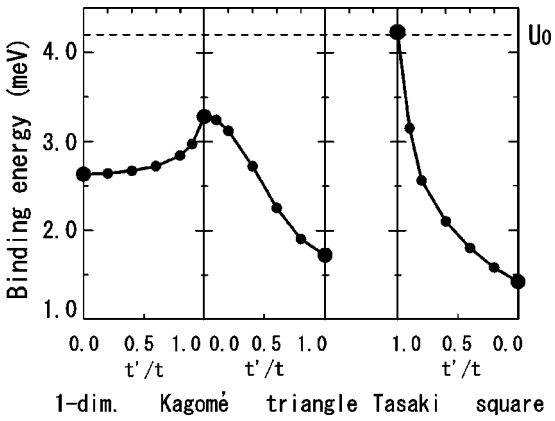

FIG. 4. Calculated binding energies of excitons for various lattices. Transfer energy t' which corresponds to the carrier transfer along broken lines shown in Figs. 2(a) and 2(b), is continuously changed from $t'=0$ to $t'=t=t^e=t^h$, yielding the gradual modification from the one-dimensional and Kagomé lattices to the Kagomé and triangle lattices, respectively. Calculations are performed for the 15×15 unit cells.

It should be noted here that when we introduce another transfer energy t' shown by broken lines in Figs. 2(a) and 2(b), the triangle and Kagomé lattices are obtained from the Kagomé and one-dimensional lattices, respectively, by changing t' from $t'=0$ to $t'=t^e=t^h$. This treatment enables us to study the effect of the continuous dimensional change of a lattice from a one-dimensional lattice to a two-dimensional triangle lattice by way of a Kagomé lattice.

Figure 4 shows the calculated binding energies of excitons for various lattices. It is seen that the exciton binding energies in the one-dimensional lattice are larger than those in the triangle and square lattices, which is consistent with the familiar knowledge that the exciton binding energy increases as the spatial dimension of the system decreases. However, it should be emphasized that the binding energy in the two-dimensional Kagomé lattice is larger than that in the one-dimensional lattice.

We then consider the spatial localization feature of exciton states. The calculated exciton densities are shown in Figs. 5(a)–5(d) for various lattices. In these figures, the electron is fixed on one specific site denoted by white arrows and the hole distribution is displayed. Apparently, all wave functions are *s*-like nodeless states. To evaluate the localization nature of excitons, the exciton Bohr radius is calculated by fitting the following distribution function to the exciton density shown in Fig. 5,

$$P_h(\mathbf{r}) = P_0 \exp\left[-\frac{2|\mathbf{r}-\mathbf{r}_e|}{\xi}\right]. \tag{4}$$

Here, $\mathbf{r}_e$ is the coordinate of the fixed electron and ξ is the exciton radius.

The calculated exciton radiuses are 102, 42, 36, and 108 nm for the one-dimensional, Kagomé, triangle, and square lattices, respectively. Therefore, the excitons are localized in the Kagomé lattice as compared to the one-dimensional and square lattices, which is one of the reasons for the large

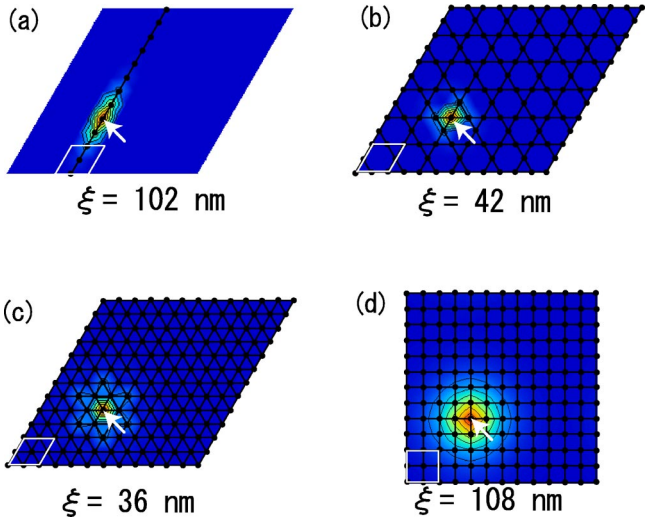

FIG. 5. Calculated exciton densities for various lattices. The electron is fixed on one specific site shown by white arrows and the hole spatial distribution is shown for (a) one-dimensional, (b) Kagomé, (c) triangle, and (d) square lattices. White square frames in (a)–(d) are unit cells. Calculations are performed for the 6×6 unit cells.

exciton binding energy in the Kagomé lattice because the binding energy increases as the localization increases. However, excitons in the Kagomé and triangle lattices have almost the same radii. This result indicates that the localized nature of excitons alone cannot explain why the excitons in the Kagomé lattice have larger binding energy than those in the other lattices discussed here.

The calculated exciton binding energy in the Kagomé lattice is 3.3 meV, which is larger than those in the square lattice (1.4 meV) and in bulk InAs (1.6 meV). Thus the difference of binding energy among these systems is observable in careful experiments. When one produces the Kagomé quantum-wire lattice of small size, the exciton binding energy in the Kagomé lattice becomes much larger. This is because the exciton is localized in one plaquette of the Kagomé lattice, thus weakly depending on the values of transfer energies, t^e and t^h, but the Coulomb attraction energy is roughly proportional to the inverse of the lattice constant a. When a is around 6 nm, the binding energy is estimated as 18 meV. On the other hand, the excitons in other lattices are sufficiently extended that their energies weakly depend on the value of a. Thus, it is expected that as the lattice size decreases, the exciton-energy difference between the Kagomé and other lattices increases.

B. Another flat-band system: Tasaki lattice

Next, we consider the exciton states in another flat-band system, i.e., the Tasaki lattice, which is shown in Fig. 6(a).[12] The band structure of the Tasaki lattice is shown in Fig. 6(b). The flat bands appear as the bottom conduction band and the top valence band. The exciton state in the Tasaki lattice is calculated in a similar way to those in the other lattices given in the preceding section. The calculated binding energy is also shown in Fig. 4.

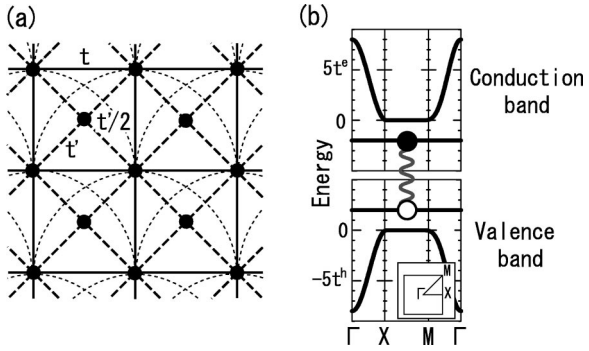

FIG. 6. (a) Schematic diagram of the Tasaki lattice. In this lattice, the transfer energies of an electron and a hole are t between two sites, which are connected by straight solid lines, while the transfer energies are t' between two sites connected by straight broken lines. The transfer energies represented by broken circular lines are $t'/2$. When $t'=0$, the lattice corresponds to the square lattice. On the other hand, when $t'=t$, the original Tasaki lattice is obtained. (b) The electronic band structure of the Tasaki lattice with $t'=t$.

It is seen that the binding energy in the Tasaki lattice (4.2 meV) is much larger than that in the Kagomé lattice (3.3 meV). This is because, as shown in Fig. 6(b), the Tasaki lattice has the full band gaps between the flat bands and the other bands, and thus, the localizations of an electron and a hole state in the flat band are stronger compared to the case of the Kagomé lattice. It should be noted here that the exciton binding energy is larger than even the on-site Coulomb attraction energy of $U_0=4.18$ meV. Note that U_0 is the maximum value of the Coulomb attraction energy for the case of one-site localization of both an electron and a hole. This result clearly indicates that the localized nature of flat-band states is not the unique origin of larger exciton binding energy.

C. Perturbation analysis of flat-band exciton

To clarify the origin of the large binding energy of an exciton in the flat-band lattice system, we perform the perturbation calculations of exciton states using the finite system. The Coulomb attraction interaction, the third term in Eq. (1), is treated as the perturbation, $\hat{W}$. For simplicity, we assume that the interaction is of short range and works only at the same site as $U(r_{ij})=-U_0\delta_{ij}$. Moreover, the 2×2 finite Kagomé lattice with the periodic boundary condition is used, together with the corresponding-size square lattice for comparison.

In the case of the square lattice, the lowest eigenstate of an electron $|\phi^{(e)}\rangle$ or a hole $|\phi^{(h)}\rangle$ is the linear combination of the i-site localized states, $|i\rangle$, with the same-magnitude coefficients, C_i, as $|\phi^{(e)}\rangle=\Sigma_i C_i|i\rangle$, where the sign of C_i is given as shown in Fig. 7(a). Remember that the electron and hole transfer energies have positive values in this paper, and thus, that coefficients of nearest-neighbor sites have different signs. The unperturbed exciton eigenstate is the tensor product of these states as

$$|\Psi^{(0)}\rangle=|\phi^{(e)}\rangle|\phi^{(h)}\rangle. \tag{5}$$

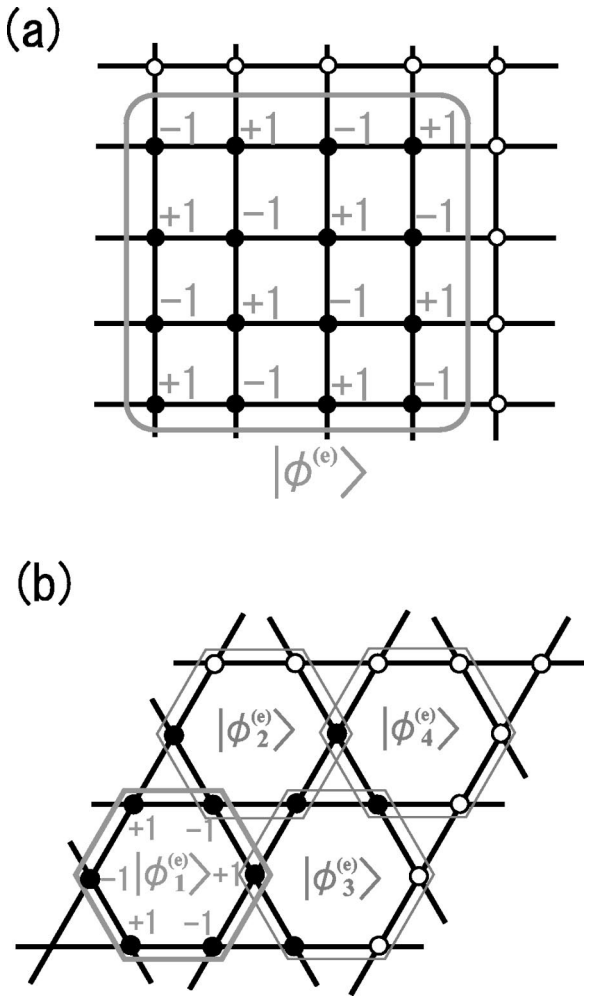

FIG. 7. Schematic of the lowest eigenstates of a conduction-band electron or a valence-band hole: (a) square and (b) Kagomé lattices. The frames (gray lines) display the localization regions of eigenstates and the inserted numbers on the sites, $+1$ and -1, represent the amplitudes of eigenfunctions. In the case of the Kagomé lattice, the lowest eigenstates are degenerate as shown by $|\phi_1^{(e)}\rangle$ to $|\phi_4^{(e)}\rangle$.

Then, the first-order perturbation gives the binding energy of exciton $E_B^{(1)}$ as

$$E_B^{(1)} = -\langle \Psi^{(0)} | \hat{W} | \Psi^{(0)} \rangle \tag{6}$$

$$= +\frac{1}{16} U_0, \tag{7}$$

where the value of denominator, 16, corresponds to the number of the lattice points in Fig. 7(a), and reflects the extended nature of electron and hole band states.

In the case of the Kagomé lattice, it is well known that the lowest eigenstates of an electron $|\phi_i^{(e)}\rangle$ and a hole $|\phi_i^{(h)}\rangle$ are the linear combinations of the localized states around hexagonal plaquettes, respectively, as shown in Fig. 7(b).[3] Namely, the site coefficients have the same magnitudes and possess the signs as shown in Fig. 7(b). Since there are four plaquettes in the present 2×2 lattice, both the eigenstates, $|\phi_i^{(e)}\rangle$ and $|\phi_i^{(h)}\rangle$, are fourfold degenerated with $i,j=1$–4, which is the origin of flat bands. Since these localized states produce complete sets of flat bands, the unperturbed eigenstates are given by

$$|\Psi_{(i,j)}^{(0)}\rangle = |\phi_i^{(e)}\rangle |\phi_j^{(h)}\rangle, \tag{8}$$

which are 16-fold degenerated. Since these states are nonorthogonal, i.e., overlap each other, we have to apply the degenerate nonorthogonal first-order perturbation to estimate the exciton binding energy, $E_B^{(1)}$, as follows:

$$\sum_{\alpha=1}^{16} C_\alpha \langle \Psi_\beta^{(0)} | W | \Psi_\alpha^{(0)} \rangle = -E_B^{(1)} \sum_{\alpha=1}^{16} C_\alpha \langle \Psi_\beta^{(0)} | \Psi_\alpha^{(0)} \rangle. \tag{9}$$

Here, α denotes the basis pair, (i,j).

One can classify the matrix elements in Eq. (9) into three groups reflecting the physical characteristics of flat-band states: (i) The diagonal matrix elements of the left-hand side reflect the localized nature of flat-band eigenstates, because $\langle \Psi_\alpha^{(0)} | \hat{W} | \Psi_\alpha^{(0)} \rangle$ is the simple average of the Coulomb interaction by the single state, $|\Psi_\alpha^{(0)}\rangle$, similar to Eq. (6). (ii) The nonzero off-diagonal matrix elements have the values of $\pm U_0/18$ and appear due to the degeneracy of flat-band states, similar to the case of the usual degenerate perturbation. On the other hand, (iii) the off-diagonal matrix elements of the right-band side reflect the nonorthogonal (overlap) nature of flat-band states. To clarify the contributions of these three groups of the matrix elements to the exotic exciton state, we multiply off-diagonal matrix elements of a group (ii) by the factor η and those of a group (iii) by the factor ξ. The solution of thus modified Eq. (9) gives the exciton binding energy as

$$E_B^{(1)} = \frac{2(2+2\eta+\sqrt{1+2\eta+13\eta^2})}{4(9+4\xi)} U_0. \tag{10}$$

In the case of $\eta=\xi=0$, which corresponds to the case of neglecting both the nonorthogonality and the degeneracy but considering only the localized nature of flat-band states, $E_B^{(1)}=2U_0/12$. This value is larger than that of the square lattice, which indicates that the exciton in the Kagomé lattice is more localized than that in the square lattice and is consistent with the results of numerical calculation presented previously. We then switch on the factors, η and ξ, step by step as displayed in Fig. 8. When we change the value of ξ from 0 to 1, which corresponds to the case considering the nonorthogonality and the localized nature of flat-band states, $E_B^{(1)}$ decreases to $U_0/12$. This is because the nonorthogonality induces the extension of the localized flat-band states and gives the loss of attractive Coulomb energy. When both η and ξ have the values of 1, corresponding to the case considering not only the localization and nonorthogonal natures but also the degeneracy of flat-band states, $E_B^{(1)}$ again increases to $3U_0/12$. From this analysis, we can clearly conclude that not only the localization nature, but also the degeneracy of the flat-band eigenstates, is essential origin to enlarge the binding energy of flat-band exciton.

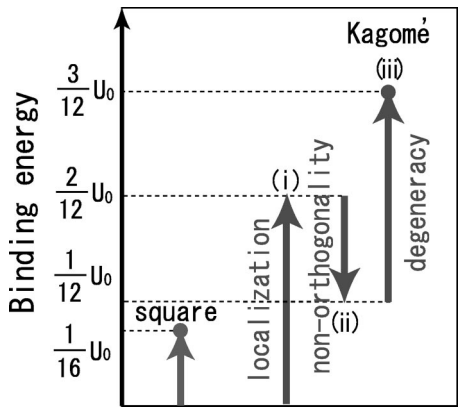

FIG. 8. Schematic diagram representing contributions to exciton binding energy by the present step-by-step perturbation analysis. (i) localization contribution, (ii) nonorthogonality (overlap) contribution, and (iii) degeneracy contribution. In case of square lattice, only the localization contribution exists.

D. Magnetic-field effect

Here, we consider the exciton binding-energy variation when the magnetic field is applied perpendicular to the lattice surface. In the tight-binding model, the magnetic-field effect is introduced into the Hamiltonian by multiplying the transfer energy t_{ij} by the phase factor,[13]

$$t_{ij} \cdot \exp\left[i \frac{2\pi e}{hc} \int_{\mathbf{r}_i}^{\mathbf{r}_j} \mathbf{A}(\mathbf{r}) d\mathbf{r} \right], \tag{11}$$

where $\mathbf{A}(\mathbf{r})$ is the vector potential, and $\mathbf{r}_i$ is the position vectors of the ith site.

Figure 9 shows the calculated exciton binding energies for various lattices as a function of the magnetic field. Here, in the case of 3.7 T, fourfold unit magnetic fluxes are included in the unit cell of the Kagomé lattice. The schematic band structures in the cases of the magnetic fields of -3.7, 0, and 3.7 T, without the Coulomb attraction interaction, are also shown in the upper panels of Fig. 9. In general, the magnetic field bends the flat-band dispersions and changes the position of flat bands. It is seen in Fig. 9 that the binding energy of an exciton in the Kagomé lattice suddenly decreases with applying the magnetic field and that its magnitude becomes comparable to those in other two-dimensional lattices. This result indicates that the large exciton binding energy is obtained only when the flat bands appears as the lowest-conduction and highest-valence bands. Moreover, from this result, we can say that in the Kagomé lattice, one can largely control the binding energy of excitons by applying a magnetic field.

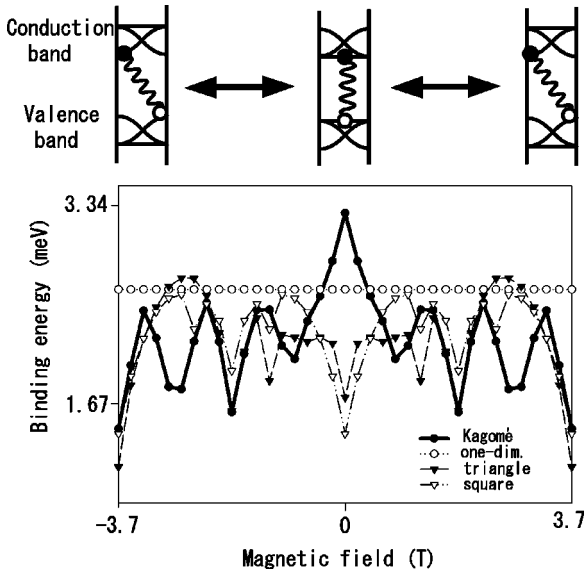

FIG. 9. Calculated exciton binding energies of various lattices as a function of the magnetic field perpendicular to the lattice plane. Upper panels show the schematic band structures of the Kagomé lattice, in the cases of -3.7 T, 0 T, and 3.7 T from the left to the right. Calculations are performed for the 15×15 unit cells.

Finally, we comment on the sign of electron and hole transfer energies. As shown in the upper pictures of Fig. 9, an electron and a hole transfer energies in the case of ± 3.7 T are $-t^e$ and $-t^h$, respectively, while those in the case of 0 T are t^e and t^h. In this way, we can change the sign of carrier transfer energies by applying an external magnetic field. This is the reason why we take t^e and t^h as positive in the present paper.

E. Exciton complexes

Since the radius of an exciton is small in the Kagomé lattice, it is expected that when highly excited, this system realizes the high-density states of excitons instead of realizing the exciton complexes, the electron-hole liquid droplet, and the electron-hole plasma states. To study this possibility, we consider the stability of exciton against the production of exciton complexes, by calculating the binding energies of charged exciton and biexciton, which are bounded states made of two electrons and one hole, and two electrons and two holes, respectively.

The following Coulomb repulsive interactions between electrons or holes are added to the Hamiltonian of Eq. (1),

$$U^{ee}(r_{ij}) = U^{hh}(r_{ij}) = \begin{cases} +U_0 & \text{for} \quad i=j \\ +\dfrac{0.75U_0}{(r_{ij}/a)} & \text{for} \quad i\neq j, \end{cases} \tag{12}$$

where r_{ij} is the distance between two electrons or two holes. The binding energies of exciton complexes are calculated similarly, by taking into account the antisymmetry of wave functions for the exchange between two electrons or two holes. Here, the binding energy of a charged exciton is defined as the energy required to decompose into an exciton and a free hole, while the binding energy of biexciton is also defined as the energy required to decompose into two excitons.

We calculated the binding energies of an exciton, a charged exciton with the total spin $S=1/2$ and 3/2, and a biexciton with $S=0$, 1, and 2, and found that the lowest-spin states, $S=1/2$, and $S=0$, are most stable for the charged exciton and biexciton, respectively. Figure 10 shows the calculated results of the exciton and the lowest-spin states for a charged exciton and biexciton for various lattices. It is seen

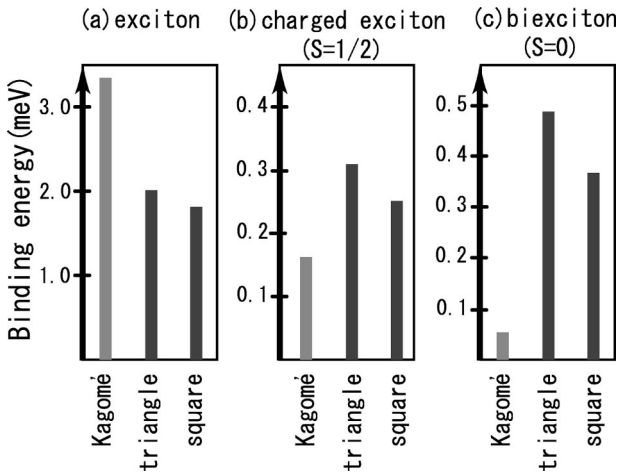

FIG. 10. Calculated binding energies for triangle, Kagomé, and square lattices: (a) exciton, (b) charged exciton, and (c) biexciton. Calculations are performed for the 3×3 unit cells.

that the binding energy of an exciton in the Kagomé lattice is much larger than those in other two-dimensional lattices, while the binding energies of a charged exciton and biexciton in the Kagomé lattice are much smaller than those in the triangle and square lattices. Therefore, one can conclude that the charged exciton and biexciton are less stable in the Kagomé lattice as compared to the other lattices.

IV. SUMMARY

The flat-band exciton in the InAs Kagomé quantum-wire system was studied employing a tight-binding model. It was found that the binding energies of flat-band excitons in the Kagomé and Tasaki lattices are much larger than those in other two-dimensional lattices and even larger than that in the one-dimensional lattice. By the perturbation analysis, it was shown that both the localized nature and the macroscopic degree of degeneracy of the flat-band eigenstates of electron and hole are the origins of large exciton binding energy. It was also found that when the magnetic field is applied, the binding energy of a flat-band exciton shows a large variation. In the Kagomé lattice, a charged exciton and a biexciton have smaller binding energies as compared to those in other lattices.

ACKNOWLEDGMENTS

This work was supported by the Ministry of Education, Culture, Sports, Science, and Technology, Japan. We thank the Super Computer Center, ISSP, University of Tokyo for the use of SR8000.

*Email address: ishii@physics.s.chiba-u.ac.jp
†Email address: nakayama@physics.s.chiba-u.ac.jp
‡Email address: jay@cfs.chiba-u.ac.jp

[1] D. Hofstader, Phys. Rev. B **14**, 2239 (1976).
[2] C. Albrecht, J.H. Smet, K. von Klizing, D. Weiss, V. Umansky, and H. Schweizer, Phys. Rev. Lett. **86**, 147 (2001).
[3] A. Mielke, J. Phys. A **25**, 4335 (1992).
[4] A. Mielke and H. Tasaki, Commun. Math. Phys. **158**, 341 (1993).
[5] K. Shiraishi, H. Tamura, and H. Takayanagi, Appl. Phys. Lett. **78**, 3702 (2001).
[6] P. Mohan, F. Nakajima, M. Akabori, J. Motohisa, and T. Fukui, Appl. Phys. Lett. **83**, 689 (2003).
[7] H. Ishii, T. Nakayama, and J. Inoue, Surf. Sci. **514**, 206 (2002).
[8] H. Ishii, T. Nakayama, and J. Inoue, in *Proceedings of the 26th International Conference on the Physics of Semiconductors, Edinburgh, 2002*, edited by A. R. Long and J. H. Davies (Institute of Physics, Bristol, UK and Philadelphia, 2003).
[9] K. Shiraishi, H. Tamura, and H. Takayanagi (unpubished).
[10] K. Ishida, Phys. Rev. B **49**, 5541 (1994).
[11] K. Ishida, H. Aoki, and T. Chikyu, Phys. Rev. B **47**, 7594 (1993).
[12] K. Kusakabe and H. Aoki, Phys. Rev. Lett. **72**, 144 (1994).
[13] Y. Hasegawa, Y. Hatsugai, M. Kohmoto, and G. Montambaux, Phys. Rev. B **41**, 9174 (1990).